Passive microwave signatures of autumnal sea ice types from ship-based observation

Byong Jun Hwang, Jens K. Ehn, Ryan Galley, and David G. Barber
Centre for Earth Observation Science
University of Manitoba
Winnipeg, MB, Canada
Email: umhwangb@cc.umanitoba.ca

***Abstract*—Surface-scale passive microwave signatures of newly formed sea ice were collected using ship-based radiometers in the Southern Beaufort Sea and Amundsen Gulf between mid October and mid November 2003. Sea ice in the region was highly spatially and temporally variable. Over a heterogeneous area of open water and thin ice, polarization ratios showed multimodal frequency distributions and the differences between surface and satellite radiometric data were large. However, differences were small over a homogeneous area of snow-covered first-year ice during late fall and the corresponding histograms showed unimodal distributions. Our results suggest that sub-pixel heterogeneity is a critical factor in characterizing the mixture rules used in passive microwave sea ice algorithms.**

Keywords -sea ice; spatial heterogeneity; microwave; radiometry;

I. INTRODUCTION

In passive microwave sea ice algorithms, remotely sensed brightness temperature (T_B) is typically expressed as an incoherent linear combination of fractional contributions from two (open water and sea ice) or three surface types (open water, first-year and multiyear ice) (see [1], [2] and [3]). However, spatial heterogeneity within the footprint of space-borne microwave sensors (hereinafter called sub-pixel heterogeneity) is one of the limiting factors in retrieving sea ice thermophysical state information using satellite microwave radiometry. The problem occurs mainly in the fall freeze-up and spring/summer melt periods in time and within sea ice margins spatially. No algorithm satisfactorily resolves heterogeneous pixels near the ice edge [4] and heterogeneous areas of open water and thicker ice were not distinguishable from a homogenous thin ice area using microwave radiometry [5].

The presence of a mixture of new, thin sea ice types has been a major problem in the retrieval of sea ice concentration from remotely sensed passive microwave radiometry (e.g., [6] and [7]). Thin sea ice types are highly variable in time and space during the fall freeze-up. Surface-scale radiometric measurements of thin ice types are relatively rare in the literature; however, they are critical in addressing the impact of sub-pixel heterogeneity on satellite-scale radiometry.

Here we present surface-scale radiometric data over newly formed sea ice collected from a ship-based radiometer system during the fall period and use these data in an attempt to address the sub-pixel problem. First we present the statistical characteristics of the observed surface-scale radiometric measurements, and then we compare the observed surface radiometry with satellite-scale data. Finally we discuss the impact of sub-pixel variability on the mixing rules in describing satellite radiometry.

II. FIELD OBSERVATION AND DATA

A. Ship-based measurement

Ship-based observations were conducted from October 18 to November 13, 2003, in the Southern Beaufort Sea and Amundsen Gulf in the Northwest Territories, Canada, as a part of the Canadian Arctic Shelf Exchange Study (CASES) fall field program (Figure 1).

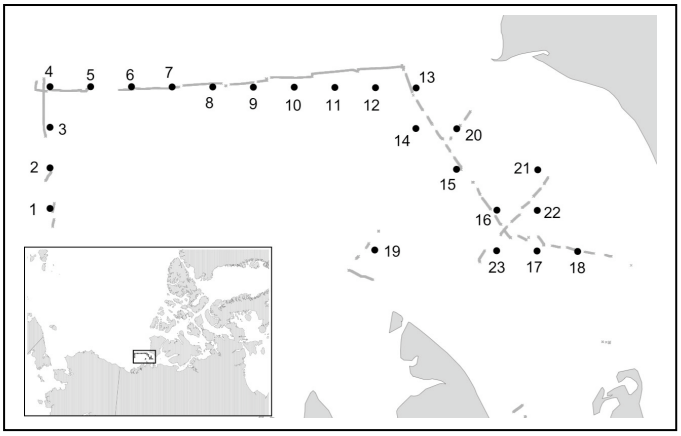

Figure 1. Map of study region. The numbers in the map indicate the nearest SSM/I pixel centers to surface data. These pixel numbers are consistently used in this study

Dual polarized (vertical and horizontal) microwave radiometers at 19, 37 and 85 GHz were mounted about 12 m above sea level onboard research icebreaker Canadian Coast Guard Ship *CCGS Amundsen*. A web camera was used to continuously photograph the sea surface within the radiometers field-of-view. Microwave measurements were taken both at oceanographic station stops and during transit between stations. A detailed study addressing measurements conducted on

station has been completed (see [8]). Here the focus is on transit measurements relying on surface photographs and notes taken during transit measurements to infer ice type and surface condition. During transit, the radiometers were fixed at a 53-degree incident angle and were programmed to sample at 5-second intervals. The high frequency sampling conducted during transit provides relevant and needed information regarding small-scale variability (~meters) in passive microwave signatures.

The study region was categorized into five characteristic areas according to ice conditions observed onboard the icebreaker, i.e., NI, YI, PAN, FY and MY. NI characterizes a heterogeneous area of open water and thin nilas. NI occurred between pixel 13 and pixel 18 in Amundsen Gulf during the second week of experiment (see Figure 1). Grey and grey-white ice (YI) was frequently observed in pixels 1-3, pixel 6-7 and pixels 11-12 (Figure 1). Between pixel 8 and pixel 10, we frequently observed consolidated pancake ice (PAN) (Figure 1). Near pixels 4 and 5, the icebreaker was located adjacent to multiyear ice pack boundary (MY) (Figure 1). Snow covered first-year ice (FY) occurred between pixels 19 and 23 (Figure 1).

B. SSM/I data

SSM/I daily averaged T_B data [9] were obtained from the National Snow and Ice Data Center for October 18 – November 13, 2003. Data points from the surface-based observations within a radius of 12.5 km of the nearest SSM/I pixel were used for comparisons (see section III).

C. Definition of ratios

Polarization ratios (PRs) and spectral gradient ratios (GRVs) were calculated:

$$PR(\nu) = [T_B(\nu V)-T_B(\nu H)]/[T_B(\nu V)+T_B(\nu H)] \quad (1)$$

$$GRV(\nu_1, \nu_2) = [T_B(\nu_1 V)-T_B(\nu_2 V)]/[T_B(\nu_1 V)+T_B(\nu_2 V)] \quad (2)$$

$$DPR(\nu_1, \nu_2) = PR(\nu_1)-PR(\nu_2) \quad (3)$$

where ν is frequency (GHz), and V and H denotes vertical and horizontal polarizations, respectively. In sea ice algorithms, SSM/I ratios ($R_{SSM/I}$) are depicted as weighted sum of surface-scale ratios (R_{surf}). The absolute difference between $R_{SSM/I}$ and R_{surf} (ΔR) is expressed by

$$\Delta R = | R_{SSM/I} - \sum^{N} [(f_i / N) \times R_{surf}(i)] | \quad (4)$$

where, f is histogram counts for each bin (i) and N is total counts. The linear mixture rule is more valid when ΔR is smaller.

III. RESULTS AND DISCUSSIONS

A. Surface-scale radiometry

Ship-based in-situ microwave signatures show considerable variability in both space and time (Figure 2). The PR(19) frequency distribution for all data points shows three peaks at about 0.05, 0.09 and 0.28 (Figure 3a). Stationary observations showed that these three peaks represent thin snow covered young ice, bare nilas or young ice and open water respectively [8]. Therefore, the highest PR(19) peak at about 0.05 suggests that thin snow-covered young ice occurred most frequently during the experiment. This agrees with visual observations of ice conditions onboard the icebreaker.

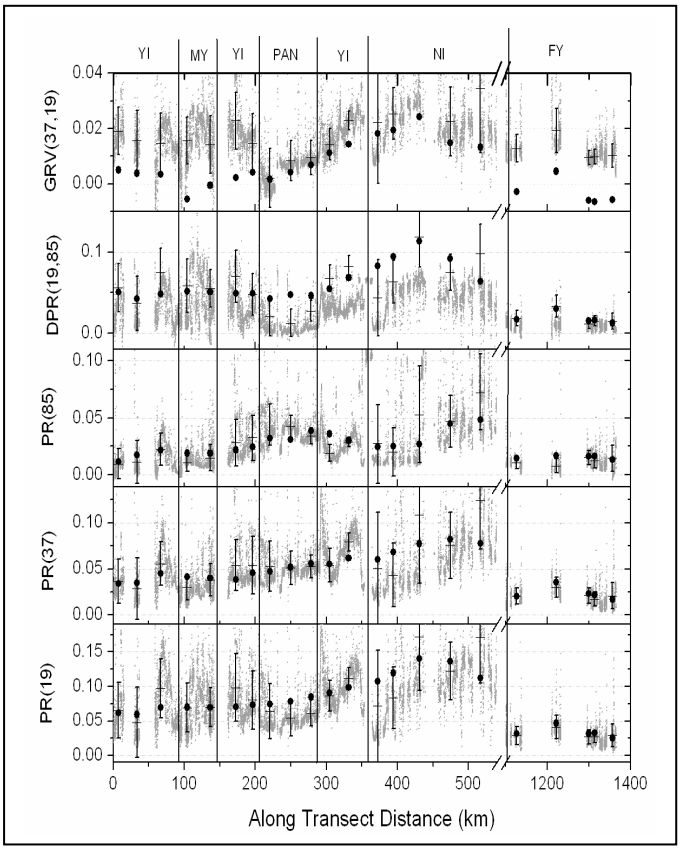

Figure 2. Surface-scale microwave radiometry according to the along-transect distance. Small grey dots are 10-m avearged data points of surface radiometry. Horizontal bars with error bars are the means of surface data within 12.5 km radius of the nearest SSM/I pixel. The Y-error bar indicates one standard deviation. Large black dots are the SSM/I values of the nearest pixel. The polarization and spectral gradient ratios in the figure were defined in section II.

The variability of microwave signatures is characterized according to the five typical areas. Largest average surface PR(19) (0.124) occurred in the NI area where mostly open water and thin nilas were observed (Table I). The corresponding histogram of the NI area shows three distinctive PR(19) peaks at about 0.05, 0.11 0.28 (Figure. 3b). The locations of these peaks are close to those in the histogram for all data (Figure 3), however, the highest PR(19) frequency occurs at ~0.11. This indicates larger thin nilas ice coverage within that area.

The second largest average PR(19) (0.084) occurred in the YI area (Table I). The corresponding histogram shows only one distinctive PR(19) peak at about 0.07 (Figure 3c) which is close to the lower limit of bare ice [8]. This indicates more frequent occurrence of thin snow covered young ice. The third

largest average PR(19) occurred in the MY area. The corresponding histogram shows one peak that is similar to the YI area but more inclined toward lower values (Figure 3d). This inclination is attributed to large concentration of multiyear ice within that area.

TABLE I. MEAN AND STANDARD DEVIATIONS OF SURFACE PR(19) AND OF THE DIFFERENCE BETWEEN SURFACE AND SSM/I PR(19)S.

Area	Surface PR(19)	Surface PR(19) – SSM/I PR(19)
NI	0.124±0.042	0.032±0.017
YI	0.084±0.022	0.013±0.010
PAN	0.060±0.005	0.019±0.007
FY	0.031±0.007	0.005±0.001
MY	0.079±0.000	0.001±0.000

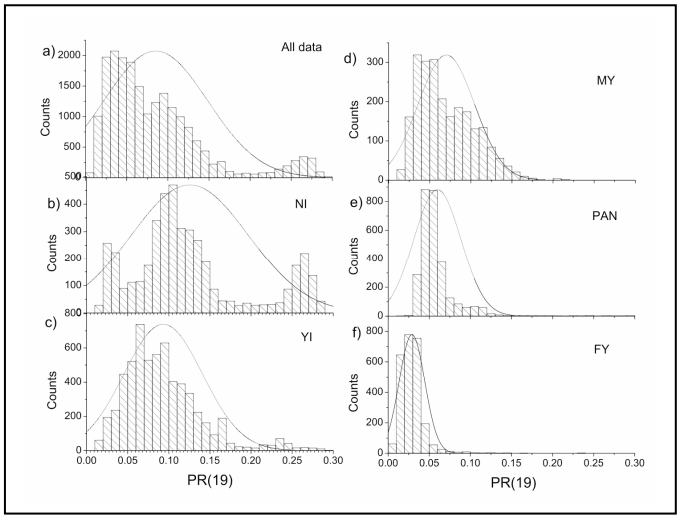

Figure 3. Frequency distributions of PR(19) for all data points, NI, YI, PAN, FY and MY areas. The curve in a solid line is Gaussian distribution.

Average PR(19) in the PAN area is 0.060, the fourth largest average PR(19) (Table I). The corresponding frequency distribution is very distinctive; most of the data points (~60%) are located between 0.04 and 0.06 (see Figure 3e). The histograms for PR(37) and PR(85) also show a similar shape and peaks (not shown here) resulting in very small DPR(19,85) or DPR(19,37) values (Figure 2). This unique microwave signature over consolidated pancake ice was also observed during stationary measurements [8]. Figure 4 shows surface photographs of some of the consolidated pancake ice encountered in the PAN area. This ice type is common in the Southern Ocean and characterized by lower bulk salinity than surrounding frazil nilas and elevated rims on the outer boundaries of the pancakes [10]. However it has been less frequently observed in the Arctic Ocean.

The smallest average PR(19) (=0.031) occurs in FY area (Table I). In FY area most of the PR(19) data points (~80%) are located between 0.015 and 0.045 (Figure 3f). This indicates that the area consisted of a homogeneous surface of thick snow covered ice. The frequency distribution comes close to a unimodal distribution within the area where the average PR(19) is smaller. However, in the NI area the histogram is a multimodal distribution.

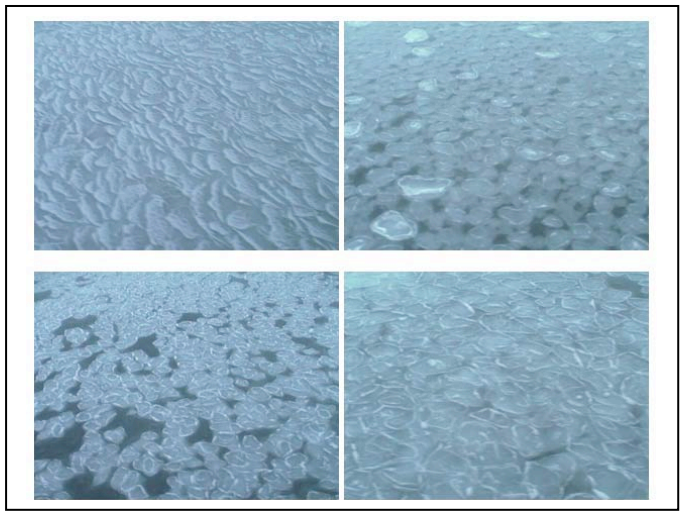

Figure 4. Surface photography of consolidated pancake ice frequently encountered in 'PAN' area.

B. Comparison with SSM/I radiometry

We only present PR(19) in addressing the differences between surface and SSM/I radiometry because 19 GHz is less affected by the atmosphere compared to 37 and 85 GHz. The average differences between mean surface and SSM/I PR(19)s vary between 0.001 and 0.032 (Table I). The small average differences occur in the FY and MY areas, which show unimodal frequency distributions (see Figure 3d and f). The large average differences occur in the NI and PAN areas. The NI area shows a trimodal distribution, but the PAN area shows a unimodal distribution.

For each SSM/I pixel, the four smallest differences between surface and SSM/I PR(19)s occur in pixels 1, 4, 5 and 20 (Figure 2). The corresponding differences are 0.004, 0.001, 0.001 and 0.003. For these cases, the histograms are close to unimodal distributions (Figure 5). The four largest differences occur in pixels 13-15 and 17 within the NI area (see Figure 2). The corresponding differences are 0.036, 0.036, 0.032 and 0.058 respectively. Three of the four histograms show strongly bi-modal frequency distributions (Figure 6). In SSM/I NASA Team algorithm [11], the four smallest differences in PR(19) result in only a difference of 0-3% in sea ice concentrations. However, the four largest differences in PR(19) result in a difference of 9-20% in sea ice concentrations.

It should, however, be noted that surface radiometry does not completely cover the entire footprint of SSM/I. For pixel 15, large numbers of surface data points adjacent to the nearest SSM/I grid were missing (Figure 1). Thus, the surface PR(19) shown in Figure 6b may not be statistically representative of the average within the SSM/I footprint. Furthermore, the area defined by a 12.5-km radius does not exactly match the SSM/I footprint at 19 GHz. However, daily SSM/I T_B data were averaged into a 25-km grid. Using larger than 12.5-km radius causes overlapping between neighboring pixels and become statistically less robust in comparing statistics of surface

signatures for individual pixel. It should also be noted that the daily averaged SSM/I T_Bs do not exactly match the timing of surface radiometry measurements. Significant changes in sea ice within a day may affect the difference between surface and SSM/I PR(19)s.

Within PAN areas, surface PR(19)s were well defined around 0.05 with very little variability. SSM/I PR(19)s in PAN area show values higher by about 0.023 and the corresponding DPR(19,85) is higher (Figure 2), and SSM/I GRV(37,19)s are consistently smaller than those from surface observations (Figure 2). The radiometric reasons for these differences are not clear.

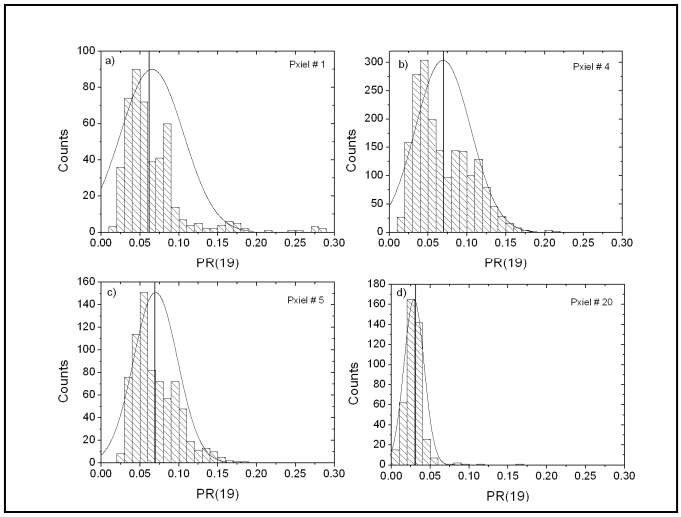

Figure 5. Frequency distributions for four smallest differences between surface and SSM/I PR(19). The curve in a solid line is a Gaussian and vertical line is the SSM/I value.

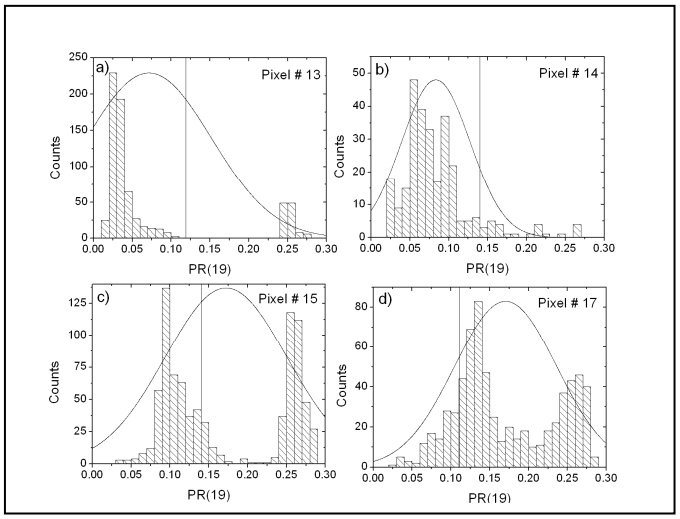

Figure 6. Frequency distributions for four largest differences between surface and SSM/I PR(19). The curve in a solid line is a Gaussian and vertical line is the SSM/I value.

IV. Conclusions

In this study, we presented ship-based radiometric observations over newly formed sea ice during the fall period. The observed microwave signatures were statistically analyzed over five typical surfaces (i.e., NI, YI, PAN, MY, FY). Results show considerable variations in observed radiometry. The largest PR(19)s occurred in NI areas where a heterogeneous mixture of open water and various thin ice surface types were typically observed. The smallest PR(19)s occurred within FY areas where homogeneous surfaces of snow covered sea ice dominated.

The observed surface microwave signatures were compared to SSM/I signatures. Results showed that differences between surface and SSM/I PR(19)s became larger over heterogeneous areas where the histograms showed multimodal distributions. This indicates that the linear mixture rule may be in question when describing satellite passive microwave signatures over a heterogeneous area.

Acknowledgment

This work was funded by NERC grants for the CASES research network, an operating grant and a Canada Research Chairs (CRC) grant, each to DBG.

References

[1] D. J. Cavalieri, P. Gloersen, and W. J. Campbell, "Determination of sea ice parameters with the Nimbus 7 SMMR", J. Geophys. Res., vol 89, 5355-5369, 1984.

[2] J. C. Comiso, "Sea ice microwave emissivities from satellite passive microwave and infrared observations", J. Geophys. Res., vol 88, 7686-7704, 1983.

[3] J. C. Comiso, "Characteristics of Arctic winter sea ice from satellite multispectral microwave observations", J. Geophys. Res., vol 91, 975-994, 1986.

[4] W. N. Meier, "Comparison of passive microwave ice concentration algorithm retrievals with AVHRR imagery in Arctic periheral seas", IEEE Geo. Trans. Rem. Sens., vol 43, no 6, 1324-1337, 2005.

[5] B. J. Hwang, and D. G. Barber, "Pixel-scale evaluation of SSM/I sea-ice algorithms in the marginal ice zone during early fall freeze-up", Hydrol. Process., vol 20, 1909-1927, 2006.

[6] T. Agnew and S. Howell, "The use of operational ice charts for evaluating passive microwave ice concentration data", Atmos. Ocean, vol. 41 no 4, 317-331, 2004.

[7] J. C. Comiso, D. J. Cavalieri, C. I. Parkinson, and P. Gloersen, "Passive microwave algorithms for sea ice concentration: a comparison of two techniques, Rem. Sens. Environ., vol 60, 357-384, 1997.

[8] B. J. Hwang, J. K. Ehn, D. G. Barber, and R. Galley, "Investigation of newly formed sea ice in the Cape Bathurst polynya: 2. Microwave emission", J. Geophys. Res., in press.

[9] J. Masianik, and J. Stroeve, "DMSP SSM/I daily polar gridded brightenss temperatures", 18 October – 13 November, 2003, Boulder, CO: National Snow and Ice Data Center, Digital media, 2007.

[10] M. J. Doble, M. D. Coon, and P. Wadhams, "Pancake ice formation in the Weddell Sea", J. Geophys. Res., vol 108, 3208, doi:10.1029/2002JC001373, 2003.

[11] D. J. Cavalieri, P. Gloersen, and W. J. Campbell, "Determination of sea ice parameters with the Nimbus 7 SMMR", J. Geophys. Res., vol 89, no D4, 5355-5369, 1984.